Efficient *Ab initio* Modeling of Random Multicomponent Alloys

Chao Jiang* and Blas P. Uberuaga†
Los Alamos National Laboratory, Los Alamos, New Mexico 87545, USA
(Received 26 November 2015; published 8 March 2016)

We present in this Letter a novel small set of ordered structures (SSOS) method that allows extremely efficient *ab initio* modeling of random multicomponent alloys. Using inverse II-III spinel oxides and equiatomic quinary bcc (so-called high entropy) alloys as examples, we demonstrate that a SSOS can achieve the same accuracy as a large supercell or a well-converged cluster expansion, but with significantly reduced computational cost. In particular, because of this efficiency, a large number of quinary alloy compositions can be quickly screened, leading to the identification of several new possible high-entropy alloy chemistries. The SSOS method developed here can be broadly useful for the rapid computational design of multicomponent materials, especially those with a large number of alloying elements, a challenging problem for other approaches.

DOI: 10.1103/PhysRevLett.116.105501

Ab initio modeling based on density functional theory (DFT) is a powerful tool that has greatly accelerated the design and discovery of materials [1–5]. The recently developed *ab initio* evolutionary methodology [6] further enables crystal structure prediction without any experimental input, making truly predictive materials design feasible. Despite its great success, extending *ab initio* calculations to multicomponent alloys exhibiting configurational disorder remains a difficult problem. To date, the three most widely used techniques for modeling disordered alloys are the single-site coherent potential approximation (CPA) [7], the special quasirandom structure (SQS) approach [8], and the "coarse-graining" cluster expansion (CE) method [9]. While CPA can elegantly treat both chemical and magnetic disorder (e.g., paramagnetic state) in random alloys at arbitrary composition, its mean-field nature limits its application to systems where local environmentally-dependent effects such as local displacements of atoms away from their ideal lattice positions are insignificant. A SQS represents the best possible periodic supercell that mimics the local pair and multisite correlation functions of a random alloy under the constraint of a given unit cell size N. Because of the $O(N^3)$ scaling of traditional DFT methods, small-unit-cell SQSs are preferred for computational efficiency. To date, SQSs with $N \leq 36$ have been successfully generated for random binary and ternary alloys [8,10–14]. However, with increasing number of alloying elements, it becomes increasingly difficult to find a small-sized SQS that can still adequately mimic the statistics of a random alloy due to the large number of correlation functions that need to be reproduced (see Fig. 1). Finally, while a CE is decidedly powerful and is capable of capturing short-range order effects at finite temperatures when used as the basis for canonical Monte Carlo simulations, the parametrization of a multicomponent CE can be computationally very expensive. To the best of our knowledge, no application of the CE technique to quaternary, quinary, and higher-order alloy systems has yet been reported in the literature.

In this Letter, motivated by the well-known Gaussian quadrature rule for numerical integration that approximates a definite integral as a weighted sum of function values at specific points, we propose to calculate a physical property f of a random alloy from a weighted average of the properties of a small set of ordered structures (SSOS) as

$$\langle f \rangle_R \approx \sum_{i=1}^{n} w_i f(\sigma_i^{\mathrm{SSOS}}), \tag{1}$$

where n is the number of structures in the set. w_i and $f(\sigma_i^{\mathrm{SSOS}})$ denote the weight and property of the ith structure in the SSOS, respectively. The weights should be positive and satisfy the normalization condition $\sum_{i=1}^{n} w_i = 1$.

To find the optimal SSOS and the corresponding weights for a given random alloy, we resort to the multicomponent CE technique [9]. For an M-component alloy containing N lattice sites, we assign a pseudospin variable S_i to each site, which can take a value between 0 and $M-1$, depending on

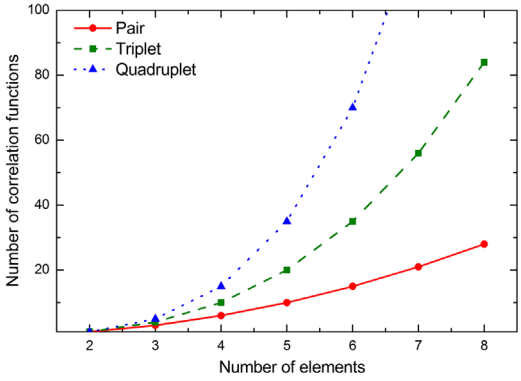

FIG. 1. Total number of correlation functions for a single cluster in high-order multicomponent alloys. Results for the nearest-neighbor pair, triplet, and quadruplet cluster in a fcc lattice are shown as a function of the number of alloying elements. Unlike in a binary alloy where the point function is unique, many distinct decorations for a cluster exist in a multicomponent alloy. For example, for an M-component alloy, there are $M(M-1)/2$ different types of decorations for each pair cluster.

which element occupies site i. The atomic arrangements on an underlying parent lattice can thus be completely characterized by the vector $\sigma = \{S_1, S_2, \ldots, S_N\}$. We further define a cluster α as a group of k lattice sites, where $k = 1, 2, 3, 4, \ldots$ indicates single-site, pair, triplet, and quadruplet clusters, etc. Formally, the dependence of a scalar property f on lattice configuration σ can be expanded as

$$f(\sigma) = J_0 + \sum_{\alpha}\sum_{s} D_{\alpha}^{s} J_{\alpha}^{s} \bar{\Phi}_{\alpha}^{s}(\sigma). \quad (2)$$

Here, the vector s is called a "decoration" that specifies the type of point function associated with each site in cluster α. $\bar{\Phi}_{\alpha}^{s}$, J_{α}^{s}, and D_{α}^{s} denote the correlation function (see Ref. [12] for detailed definition), the effective cluster interaction (ECI), and the degeneracy factor for cluster α with decoration s, respectively. J_0 is the ECI for the empty cluster. For a truly random multicomponent alloy, the ensemble average of its correlation function $\langle \bar{\Phi}_{\alpha}^{s} \rangle_R$ can be calculated analytically since there is no correlation in the occupation between various sites. We search for a SSOS and associated weights such that the weighted averages of their correlation functions match $\langle \bar{\Phi}_{\alpha}^{s} \rangle_R$ for as many clusters as possible. In the spirit of the SQS approach [8,10–14], we make a fundamental assumption that the relative importance of ECIs decreases with increasing cluster size and focus on the physically most relevant correlation functions between the first few nearest neighbors.

To generate a SSOS-$n \times N$ set that contains n ordered structures each containing N atoms per cell, we exhaustively enumerate all possible combinations of n symmetrically distinct N-atom/cell structures based on an underlying parent lattice using the ATAT code [15]. For large N, a linearly scaling numeration algorithm recently developed by Hart and Forcade [16] can be used to overcome the combinatorial explosion and the associated increase in computational time to enumerate the structures associated with larger cells. Each structure in the SSOS must have the same alloy composition as that of the alloy of interest. For computational efficiency, both n and N should be as small as possible. For each candidate set of structures, we determine their optimal weights using least-squares regression such that the periodicity error, which measures the deviation from random correlation, is minimized for a specified set of clusters under the normalization constraint:

$$\sum_{\alpha}\sum_{s}\left(\sum_{i=1}^{n} w_i \bar{\Phi}_{\alpha}^{s}(\sigma_i^{\mathrm{SSOS}}) - \langle \bar{\Phi}_{\alpha}^{s} \rangle_R\right)^2 = \min. \quad (3)$$

Among all enumerated candidate sets, the best SSOS is the one with the lowest periodicity error. The generation of a SSOS is thus an intrinsically two-step optimization process: the inner one is with respect to weights and the outer one is with respect to structure selection among a pool of small ordered structures. We note that such an optimization process may be valuable for identifying reference structures used in machine learning approaches as well.

To test the validity of the SSOS approach, we first apply it to predict the relative stability of normal versus inverse structures of $MgAl_2O_4$ and $ZnAl_2O_4$ spinel oxides [17]. In a normal II-III AB_2O_4 spinel, A^{2+} cations occupy one-eighth of the tetrahedral interstitial sites of the fcc oxygen sublattice, and B^{3+} cations occupy half of the octahedral interstices. When all the A cations exchange positions with the B cations, the spinel is referred to as "inverse." To model the inverse spinel structure in which A and B cations are randomly distributed within the octahedral (B) sublattice, we have developed a SSOS-2×28 [18] and various SQS-N structures (with $N = 28$, 56, 84, and 168 atoms per unit cell). Furthermore, we have constructed high-fidelity CEs using 17 pair, 16 triplet, and 2 quadruplet interactions by fitting to DFT calculated total energies of 146 input structures. For $MgAl_2O_4$ and $ZnAl_2O_4$, the leave-one-out cross-validation score is only 3.4 and 4.7 meV per AB_2O_4 formula unit (f.u.), respectively. The CE results are herein considered as benchmarks against which the accuracy of SSOS can be judged. For DFT calculations, we employ the all-electron projector augmented wave method [19] within the local-density approximation, as implemented in VASP [20]. To fully consider the effects of local lattice relaxations, all structures are fully relaxed with respect to both cell-internal and cell-external degrees of freedom according to quantum mechanical forces and stress tensors. More computational details can be found in the Supplemental Material [18].

Figure 2 shows the disordering energies (defined as the total energy difference between the inverse and normal configurations) of $MgAl_2O_4$ and $ZnAl_2O_4$ calculated using the SSOS, SQS, and CE methods. The ECIs of the CEs are also shown. Remarkably, by performing DFT calculations on only two 28-atom structures, our SSOS calculations give results in excellent agreement with those from the CE and the large 168-atom SQS, but with significantly lower computational cost. In contrast to metallic systems such as Nb-Mo and Ta-W [11], the slow convergence of the SQS results with respect to N observed for spinel oxides is a consequence of the long-ranged pair interactions typical of Coulomb interactions in these materials [see Figs. 2(a) and 2(b)]. It is worth noting that, compared with SQS-28, calculations using SSOS-2×28 lead to a greater than tenfold reduction in computational error for disordering energy, but with only an approximately twofold increase in computational effort. Here, by collaboratively employing several supercells of small size instead of a single large one to model the random state, the convergence with respect to cell size has been greatly accelerated, which can effectively overcome the limitation imposed by the $O(N^3)$ scaling of DFT.

As our second example, we apply the SSOS method to model the random quinary bcc alloy at the equiatomic composition, the so-called high-entropy alloys (HEAs) that have rapidly emerged as a new class of engineering materials due to their excellent physical and mechanical properties [21,22]. Remarkably, a SSOS-3×5 containing only three 5-atom/cell structures [Figs. 3(a)–3(c)] can

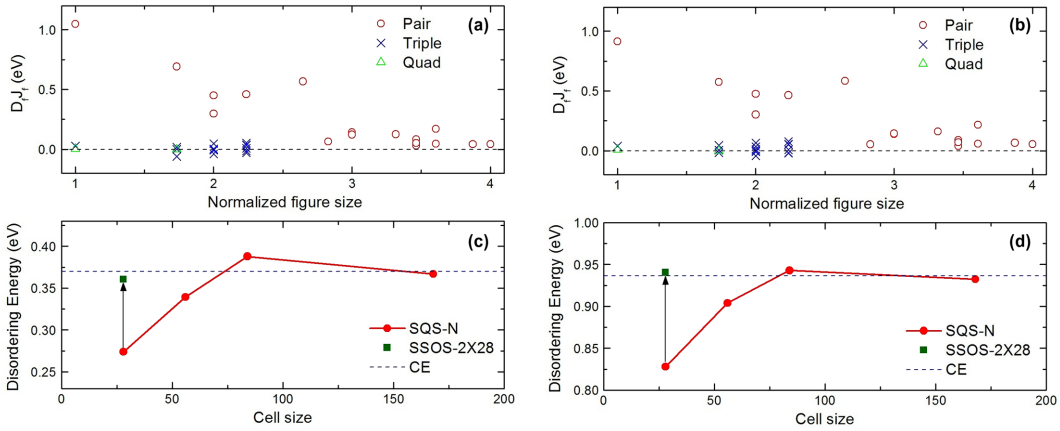

FIG. 2. Comparisons of disordering energies (eV per f.u.) of spinel oxides calculated using SSOS, SQS, and CE methods. Fitted ECIs for cation distribution in the octahedral sublattice in inverse $MgAl_2O_4$ and $ZnAl_2O_4$ are shown in (a) and (b), respectively. All figure sizes are normalized with respect to that of the of the nearest-neighbor pair. The slow-decaying pair interactions and the weak many-body (triplet and quadruplet) interactions are characteristic of Coulomb interactions. The calculated disordering energies for $MgAl_2O_4$ and $ZnAl_2O_4$ are shown in (c) and (d), respectively.

already perfectly match the 20 pair correlation functions of the random alloy for the first- and second-nearest neighbors [18]. To achieve the same level of accuracy in terms of the range of perfectly matched correlations in a single supercell, we find it necessary to use a much larger 125-atom SQS [Fig. 3(d)], which has been developed in this study using the Monte Carlo simulated annealing technique [12].

Using both the SSOS and SQS methods, we have performed DFT calculations on 12 random quinary bcc alloys using VASP [20] with PAW-PBE pseudopotentials [23]. A plane-wave cutoff energy of 341.5 eV and dense Monkhorst-Pack k-point meshes are employed to guarantee high numerical accuracy. As shown in Figs. 3(e) and 3(f), even a SSOS-3 × 5 can already provide results in excellent agreement with those obtained using a much larger 125-atom bcc SQS. The SSOS approach agrees quantitatively with SQS despite the significantly smaller computational cost of the former: the root-mean-square deviation (RMSD)

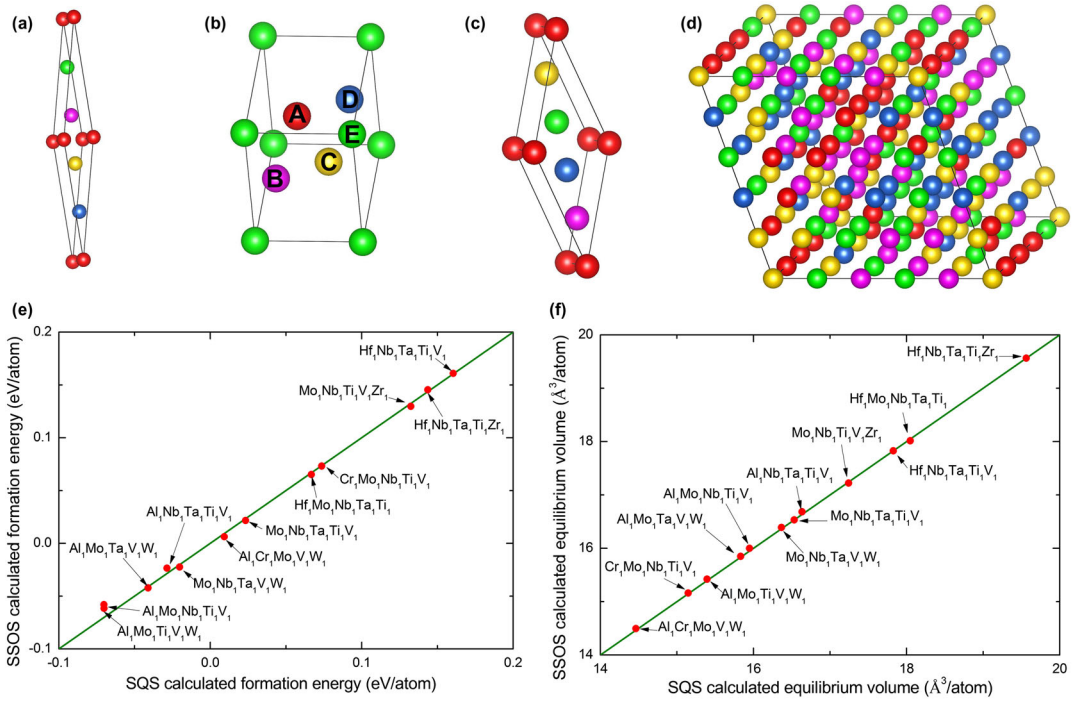

FIG. 3. Modeling the random bcc $A_1B_1C_1D_1E_1$ alloy using the SSOS and SQS approaches. The three 5-atom/cell structures σ_1^{SSOS}, σ_2^{SSOS}, and σ_3^{SSOS} in SSOS-3 × 5 are shown in (a)–(c), respectively. The 125-atom SQS structure is shown in (d). All structures are shown in their ideal, unrelaxed forms. Comparisons between SSOS calculated and SQS calculated formation energies and equilibrium volumes for 12 random bcc $A_1B_1C_1D_1E_1$ alloys are shown in (e) and (f). Only volume relaxations have been performed for this comparison. The green solid lines represent prefect agreement between the two methods.

of the formation energy and equilibrium volume of the 12 alloys is only 4.8 meV/atom and 0.028 Å^3/atom, respectively. Here, we define formation energy as the total energy difference between an alloy and the composition-weighted average of its constituent pure elements in their respective ground-state structures at $T = 0$ K.

For the comparison shown in Fig. 3, we only allow the unit cell volume to relax, with all atoms occupying their ideal bcc lattice positions. In a multicomponent solid solution, significant lattice distortion can occur due to the large size mismatch between its many constituent elements. Consequently, there can exist a large dispersion of nearest-neighbor bond lengths, the average of which corresponds to the average lattice. To further consider the effects of local lattice relaxations, we fully relax all atoms in a random bcc alloy from their ideal lattice sites into their equilibrium positions. We find that the results predicted by SSOS and SQS calculations remain in excellent agreement with each other even after full atomic relaxations (see Fig. S2 in Supplemental Material [18]). For obtaining the atomically relaxed formation energy, we estimate that the SSOS calculations are more than 40-fold faster than SQS calculations, although the RMSD between the two calculations is only 9.5 meV/atom. This good agreement confirms the suitability of using the SSOS approach for modeling local lattice relaxations in size-mismatched multicomponent alloys and predicting properties of these high-order alloys.

The combined accuracy and high computational efficiency of the SSOS method make it possible to perform high-throughput screening of the phase stability of a large number of potential bcc HEA compositions with only limited computing resources. As a demonstration of the approach, we consider all possible equiatomic quinary alloys that can be formed from the 13 elements Al, Cr, Cu, Ir, Mo, Nb, Ni, Pd, Pt, Ta, Ti, V, and W. Furthermore, all possible five combinations of the eight refractory metals Hf, Mo, Nb, Ta, Ti, V, W, and Zr are also considered. Here, we use "instability energy" [24] to measure the phase stability of a bcc HEA defined as the total energy difference between an alloy and the ground-state convex hull, which can be estimated using the Open Quantum Materials Database [25]. A large instability energy would indicate a high tendency towards ordering and thus low chance of obtaining a single-phase solid solution. Furthermore, the bcc lattice should be energetically more favorable than other competing crystal structures such as fcc. For this screening, we consider the relative lattice stability between fcc and bcc structures, each modeled using a SSOS-3 × 5 [18]. As shown in Fig. 4, our SSOS calculations correctly predict the bcc structure to be more stable for the six experimentally synthesized bcc HEAs: $Mo_1Nb_1Ta_1V_1W_1$ [26], $Hf_1Nb_1Ta_1Ti_1Zr_1$ [27], $Al_1Nb_1Ta_1Ti_1V_1$ [28], $Mo_1Nb_1Ti_1V_1Zr_1$ [29], $Al_1Mo_1Nb_1Ti_1V_1$ [30], and $Hf_1Nb_1Ti_1V_1Zr_1$ [31]. Among the 1337 HEA candidates screened, the top 2% most promising (having the lowest instability energies) bcc HEA compositions are reported

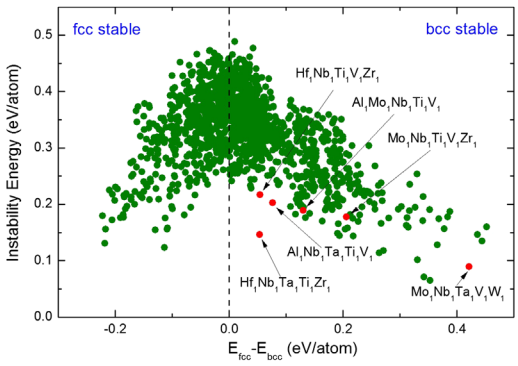

FIG. 4. High-throughput screening of potential single-phase bcc HEA compositions. Instability energy versus lattice stability plot for 1337 HEA candidates is shown. The six experimentally confirmed bcc HEA compositions are marked in red. For reasons of efficiency, only volume relaxations have been performed for this initial screening. For HEA candidates with relatively low volume relaxed instability energies, we further allow all internal atomic positions to relax in our SSOS calculations, and those results are reported in Table I.

TABLE I. The top 2% most stable single-phase bcc HEA compositions identified from the present high-throughput screening. Phase stability of HEAs is ranked according to their fully relaxed instability energies. The four experimentally verified bcc HEA compositions are shown in bold.

bcc HEAs	Instability energy (eV/atom)
$Mo_1Nb_1Ta_1Ti_1W_1$	0.046
$Mo_1Nb_1Ti_1V_1W_1$	0.048
$Mo_1Nb_1Ta_1V_1W_1$ [26]	0.068
$Hf_1Mo_1Nb_1Ti_1Zr_1$	0.081
$Mo_1Ta_1Ti_1V_1W_1$	0.081
$Mo_1Nb_1Ta_1Ti_1V_1$	0.084
$Hf_1Mo_1Nb_1Ta_1Ti_1$	0.086
$Nb_1Ta_1Ti_1V_1W_1$	0.087
$Hf_1Nb_1Ta_1Ti_1Zr_1$ [27]	0.089
$Hf_1Mo_1Nb_1Ti_1V_1$	0.092
$Hf_1Nb_1Ta_1Ti_1W_1$	0.096
$Mo_1Nb_1Ta_1Ti_1Zr_1$	0.101
$Cr_1Mo_1Ti_1V_1W_1$	0.102
$Mo_1Nb_1Ti_1V_1Zr_1$ [29]	0.102
$Cr_1Mo_1Nb_1V_1W_1$	0.104
$Nb_1Ta_1Ti_1W_1Zr_1$	0.104
$Hf_1Mo_1Nb_1Ti_1W_1$	0.113
$Al_1Mo_1Ta_1V_1W_1$	0.114
$Hf_1Mo_1Ta_1Ti_1Zr_1$	0.115
$Cr_1Mo_1Nb_1Ti_1V_1$	0.115
$Hf_1Nb_1Ti_1V_1Zr_1$ [31]	0.116
$Cr_1Mo_1Ta_1V_1W_1$	0.117
$Hf_1Mo_1Nb_1Ta_1Zr_1$	0.118
$Cr_1Nb_1Ti_1V_1W_1$	0.118
$Mo_1Nb_1Ti_1W_1Zr_1$	0.121
$Cr_1Mo_1Nb_1Ti_1W_1$	0.123
$Al_1Cr_1Mo_1V_1W_1$	0.123

in Table I. Four of them ($Mo_1Nb_1Ta_1V_1W_1$ [26], $Hf_1Nb_1Ta_1Ti_1Zr_1$ [27], $Mo_1Nb_1Ti_1V_1Zr_1$ [29], and $Hf_1Nb_1Ti_1V_1Zr_1$ [31]) have already been experimentally verified. The remaining 23 alloy compositions are thus new predictions that await experimental confirmation.

In summary, here we propose a new method to predict the properties of random multicomponent alloys using *ab initio* calculations. Instead of relying on a single large supercell to mimic the random state, we model a random alloy using a set of small ordered structures, whose weight-averaged properties approximate those of the truly random alloy. Because of the $O(N^3)$ scaling of DFT, the SSOS method has a significant advantage in terms of computational efficiency, particularly for high-order alloy systems. Using inverse AB_2O_4 spinels and random quinary bcc alloys as examples, we demonstrate that the SSOS method can predict the energetics and structural properties of random alloys in excellent agreement with those obtained using much larger supercells, even when the effects of local lattice relaxations are accounted for. Since the SSOS method relies on small cells, it allows for the possibility of high-throughput DFT calculations of high-order multicomponent systems, such as high-entropy alloys, and is ideally suited for use with more accurate but costly electronic structure approaches, such as hybrid functionals [32] and GW [33]. Finally, the SSOS approach can be used to calculate any property that can be modeled by a short-range cluster expansion, such as band gap, vibrational entropy, and bulk modulus, and thus should become a valuable tool for materials discovery of multicomponent systems.

B. P. U. acknowledges support by the U.S. Department of Energy, Office of Science, Basic Energy Sciences, Materials Sciences and Engineering Division. Los Alamos National Laboratory is operated by Los Alamos National Security, LLC, for the National Nuclear Security Administration of the (U.S.) Department of Energy under Contract No. DE-AC52-06NA25396.

*Present address: Idaho National Laboratory, Idaho Falls, Idaho 83402, USA.
chao.jiang@inl.gov
†blas@lanl.gov

[1] G. Ceder, Y.-M. Chiang, D. R. Sadoway, M. K. Aydinol, Y.-I. Jang, and B. Huang, Nature (London) **392**, 694 (1998).
[2] A. Franceschetti and A. Zunger, Nature (London) **402**, 60 (1999).
[3] G. H. Johannesson, T. Bligaard, A. V. Ruban, H. L. Skriver, K. W. Jacobsen, and J. K. Norskov, Phys. Rev. Lett. **88**, 255506 (2002).
[4] L. Vitos, P. A. Korzhavyi, and B. Johansson, Nat. Mater. **2**, 25 (2003).
[5] J. Greeley, T. F. Jaramillo, J. Bonde, I. Chorkendorff, and J. K. Norskov, Nat. Mater. **5**, 909 (2006).
[6] A. R. Oganov, J. Chen, C. Gatti, Y. Ma, Y. Ma, C. W. Glass, Z. Liu, T. Yu, O. O. Kurakevych, and V. L. Solozhenko, Nature (London) **457**, 863 (2009).
[7] B. L. Gyorffy, Phys. Rev. B **5**, 2382 (1972).
[8] A. Zunger, S. H. Wei, L. G. Ferreira, and J. E. Bernard, Phys. Rev. Lett. **65**, 353 (1990).
[9] J. M. Sanchez, F. Ducastella, and D. Gratias, Physica (Amsterdam) **128A**, 334 (1984).
[10] C. Wolverton, Acta Mater. **49**, 3129 (2001).
[11] C. Jiang, C. Wolverton, J. Sofo, L. Q. Chen, and Z. K. Liu, Phys. Rev. B **69**, 214202 (2004).
[12] C. Jiang, Acta Mater. **57**, 4716 (2009).
[13] D. Shin, A. van de Walle, Y. Wang, and Z. K. Liu, Phys. Rev. B **76**, 144204 (2007).
[14] J. E. Saal and C. Wolverton, Acta Mater. **61**, 2330 (2013).
[15] A. van de Walle, M. Asta, and G. Ceder, CALPHAD: Comput. Coupling Phase Diagrams Thermochem. **26**, 539 (2002).
[16] G. L. W. Hart and R. W. Forcade, Phys. Rev. B **77**, 224115 (2008).
[17] C. Jiang, K. E. Sickafus, C. R. Stanek, S. P. Rudin, and B. P. Uberuaga, Phys. Rev. B **86**, 024203 (2012).
[18] See Supplemental Material at http://link.aps.org/supplemental/10.1103/PhysRevLett.116.105501 for details of DFT calculations and further results for validation of the SSOS method. The detailed structural information and weighting factors of the ordered structures in the SSOSs developed in this study have also been given.
[19] G. Kresse and D. Joubert, Phys. Rev. B **59**, 1758 (1999).
[20] G. Kresse and J. Furthmuller, Phys. Rev. B **54**, 11169 (1996).
[21] J. W. Yeh, S. K. Chen, S. J. Lin, J. Y. Gan, T. S. Chin, T. T. Shun, C. H. Tsau, and S. Y. Chang, Adv. Eng. Mater. **6**, 299 (2004).
[22] P. Kozelj, S. Vrtnik, A. Jelen, S. Jazbec, Z. Jaglicic, S. Maiti, M. Feuerbacher, W. Steurer, and J. Dolinsek, Phys. Rev. Lett. **113**, 107001 (2014).
[23] J. P. Perdew, K. Burke, and M. Ernzerhof, Phys. Rev. Lett. **77**, 3865 (1996).
[24] Y. Wu, P. Lazic, P. Hautier, K. Persson, and G. Ceder, Energy Environ. Sci. **6**, 157 (2013).
[25] J. E. Saal, S. Kirklin, M. Aykol, B. Meredig, and C. Wolverton, J. Miner. Met. Mater. Soc. **65**, 1501 (2013).
[26] O. N. Senkov, G. B. Wilks, D. B. Miracle, C. P. Chuang, and P. K. Liaw, Intermetallics **18**, 1758 (2010).
[27] O. N. Senkov, J. M. Scott, S. V. Senkova, D. B. Miracle, and C. F. Woodward, J. Alloys Compd. **509**, 6043 (2011).
[28] X. Yang, Y. Zhang, and P. K. Liaw, Procedia Eng. **36**, 292 (2012).
[29] Y. Zhang, X. Yang, and P. K. Liaw, J. Miner. Met. Mater. Soc. **64**, 830 (2012).
[30] S. Y. Chen, X. Yang, K. A. Dahmen, P. K. Liaw, and Y. Zhang, Entropy **16**, 870 (2014).
[31] E. Fazakas, V. Zadorozhnyy, L. K. Varga, A. Inoue, D. V. Louzguine-Luzgin, F. Y. Tian, and L. Vitos, Int. J. Refract. Met. Hard Mater. **47**, 131 (2014).
[32] J. Heyd, G. E. Scuseria, and M. Ernzerhof, J. Chem. Phys. **118**, 8207 (2003).
[33] M. Shishkin and G. Kresse, Phys. Rev. B **75**, 235102 (2007).